

Bias-selectable tricolor tunneling quantum dot infrared photodetector for atmospheric windows

G. Ariyawansa,¹ V. Apalkov,¹ A. G. U. Perera,^{1,2,a)} S. G. Matsik,² G. Huang,³ and P. Bhattacharya³

¹Department of Physics and Astronomy, Georgia State University, Atlanta, Georgia 30303, USA

²NDP Optronics LLC, Mableton, Georgia 30126, USA

³Solid State Electronics Laboratory, Department of Electrical Engineering and Computer Science, University of Michigan, Ann Arbor, Michigan 48109-2122, USA

(Received 14 February 2008; accepted 27 February 2008; published online 19 March 2008)

A tricolor infrared detector with bias-selectable peaks based on tunneling quantum dot infrared photodetector (T-QDIP) architecture is demonstrated. Photoabsorption takes place in $\text{In}_{0.4}\text{Ga}_{0.6}\text{As}$ quantum dots (QDs) and the excited electrons are collected by resonant tunneling across an $\text{Al}_{0.2}\text{Ga}_{0.8}\text{As}/\text{In}_{0.1}\text{Ga}_{0.9}\text{As}/\text{Al}_{0.2}\text{Ga}_{0.8}\text{As}$ double barrier coupled to the QDs. The field dependent tunneling for excited carriers in T-QDIP is used to select the operating wavelength. This T-QDIP detector exhibits three distinct response peaks at $4.5/4.9 \pm 0.05$, 9.5 ± 0.05 , and $16.9 \pm 0.1 \mu\text{m}$ up to 80 K. The peak detectivity is in the range of $(1.0\text{--}6.0) \times 10^{12}$ Jones at 50 K. Bias polarity allows the selection of either the $9.5 \mu\text{m}$ or the $16.9 \mu\text{m}$ peak. © 2008 American Institute of Physics. [DOI: 10.1063/1.2898521]

Multicolor infrared (IR) detection has become an important tool in the field of IR technology due to various applications. Detecting an object's IR emission at multiple wavelengths can be used to eliminate background effects and reconstruct the object's absolute temperature. However, measuring multiple wavelength bands typically requires either multiple detectors or a single broadband detector with a filter wheel. These will require complicated detector assemblies, separate cooling systems, and numerous electronic and optical components. Consequently, such sensor systems (or imaging systems) require a complex control mechanism and hardware to achieve the fine optical alignment necessary, increasing the cost. These issues can be avoided by a single detector responding in multiple bands. Applications of multiband detectors include land-mine detection,¹ missile-warning sensors,² identification of muzzle flashes³ from firearms, and space situational awareness.⁴

Quantum dot (QD) based detectors^{5–7} have become a choice of interests for multicolor detector development. Successful research has led to the development of multicolor QD focal plane arrays.^{8–10} In order to overcome the need for external optical filters for multiband detection, several approaches have been reported. Multistack detectors¹¹ use separate electrical contacts to collect the photocurrent components generated in each active region separately. In this article, the use of applied bias to select the operating wavelength of a multicolor tunneling QD photodetector (T-QDIP) consisting of two double-barrier (DB) systems coupled to QDs is reported. Unlike the previous T-QDIP,¹² the QDs are sandwiched between two sets of DBs, allowing strong wavelength selectivity with the applied bias. A dots-in-a-well (DWELL) detector¹⁰ had two peaks, one ($\sim 5.5 \mu\text{m}$) at low bias with a second peak ($8\text{--}10 \mu\text{m}$) appearing at high bias. Both are due to transitions of carriers from QD ground state to a state in the well. In the present T-QDIP, transitions in the QDs and resonant tunneling give rise to lower dark current and a minimal spectral crosstalk with a better bias-dependent

wavelength selectivity. There is an optimum bias voltage for the response peaks, compared to “low” and “high” bias selection for the DWELL.¹⁰ Furthermore, one would expect polarization sensitivity due to the dot-to-dot transitions in this T-QDIP.

In T-QDIPs,¹² the photoexcited carriers in the QDs are collected by means of resonant tunneling^{12–14} through a DB system coupled to the QDs. Two DB systems are integrated with each QD layer and are designed such that an excited state in the QD coincides with a bound state in a DB system under certain bias conditions. The T-QDIP detector structure grown by molecular beam epitaxy (MBE) is shown in Fig. 1. The active region consists of pyramidal-shape $\text{In}_{0.4}\text{Ga}_{0.6}\text{As}$ QDs sandwiched between two DB systems that consist of an $\text{In}_{0.1}\text{Ga}_{0.9}\text{As}$ quantum well in 30 Å thick $\text{Al}_{0.2}\text{Ga}_{0.8}\text{As}$ barriers. The widths of the $\text{In}_{0.1}\text{Ga}_{0.9}\text{As}$ wells in bottom-DB (BDB) and top-DB (TDB) systems are 60 and 40 Å, respec-

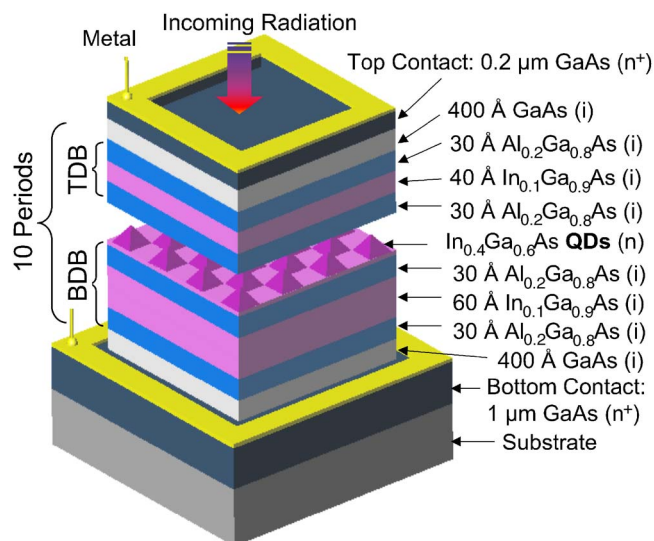


FIG. 1. (Color online) A 3D view of the processed T-QDIP structure grown by MBE. $\text{In}_{0.4}\text{Ga}_{0.6}\text{As}$ QDs are placed in between two DBs (top and bottom DBs indicated by TDB and BDB, respectively). The letter “i” indicates that the layer is intrinsic.

^{a)}Electronic mail: uperera@gsu.edu.

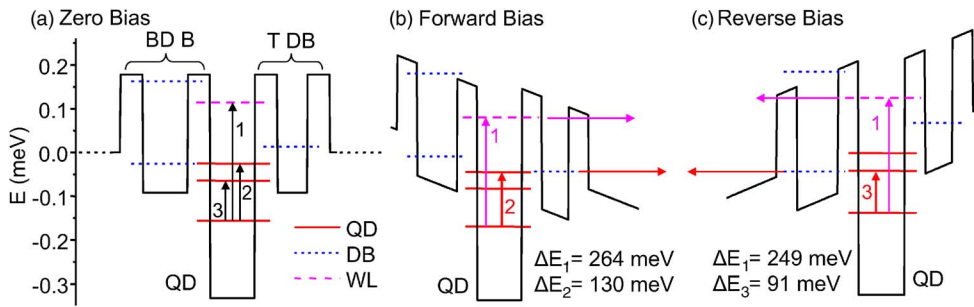


FIG. 2. (Color online) Schematic diagram of the conduction band profile of the T-QDIP structure under (a) zero, (b) forward, and (c) reverse bias conditions. The calculated bound state energies in the dots (red solid lines), wetting layer (pink dashed lines), and DBs (blue short dashed lines) are also indicated. The photoexcited carriers are collected by resonant tunneling through the DBs.

tively. There are ten periods of these QDs coupled with DBs and each period is separated with an undoped 400 Å thick GaAs layer. The GaAs and AlGaAs layers were grown at 610 °C. The $\text{In}_{0.4}\text{Ga}_{0.6}\text{As}$ QDs were grown¹⁵ at 500 °C on top of a 3 ML wetting layer. QDs with height and base dimensions of the ~ 6 and ~ 20 nm, respectively, are n -doped to $1 \times 10^{18} \text{ cm}^{-3}$ using Si as the dopant, while all other layers are undoped except the GaAs bottom- and top-contact layers (n -doped to $2 \times 10^{18} \text{ cm}^{-3}$). Vertical circular mesas for top illumination were fabricated by standard photolithography, wet chemical etching, and contact metallization techniques. The n -type top ring contact and the bottom contact were formed by evaporated Ni/Ge/Au/Ti/Au with thickness of 250/325/650/200/2000 Å. The radius of the optically active area of a processed device was 300 μm . Devices for testing were mounted on to chip carriers with silver epoxy and gold wire contacts were made from the device to the chip carrier leads.

The band structure for the reported T-QDIP detector with calculated energy levels in the QDs and DB systems is shown in Figs. 2(a)–2(c) for zero, forward (top contact is positive), and reverse (bottom contact is positive) bias conditions, respectively. The energy states in the QDs were calculated using an eight-band $\mathbf{k} \cdot \mathbf{p}$ model.¹⁶ There are three bound states located at -0.156 , -0.065 , and -0.026 eV (ground, first excited, and second excited state, respectively) with respect to the GaAs conduction band edge ($=0$ eV). The energy states in the wetting layer and the DB systems were calculated by solving the one-dimensional Schrödinger equation and the transmission probability for the DB structure was calculated using the transfer matrix method.¹⁷ The energy states in the wetting layer [purple (online) dashed line] and the DB [blue (online) short dashed lines] are also shown in Fig. 2. While these states are localized in the corresponding regions, they also can extend across the whole structure, especially the wetting layer state. As shown in Fig. 2(a), photoabsorption takes place in the QDs and electrons are excited from the QD ground state to the first QD excited state (transition 3 with $\Delta E \sim 91$ meV), to the second QD excited state (transition 2 with $\Delta E \sim 130$ meV), and to the wetting layer state (transition 1). The electric field dependent tunneling of excited carriers lead to a selectivity for photo-response peaks. Under a certain forward bias condition [see Fig. 2(b)], the second QD excited state will overlap with the state in the TDB. Hence, the carriers excited to the second QD state ($\Delta E = 130$ meV) will have the maximum tunneling probability and will be collected as the photocurrent, leading to a photoresponse at 9.5 μm . Similarly, under a certain reverse bias condition [see Fig. 2(c)], the first QD excited state will overlap with a state in the BDB leading to a response peak at 13.6 μm ($\Delta E = 91$ meV). Under both forward and

reverse bias conditions, the carriers excited to the wetting layer also can tunnel through the barriers. Hence, a short wavelength peak in the 4.5–5 μm range is also expected.

The measured and calibrated spectral response for forward and reverse bias at 50 K is shown in Fig. 3(a). Under forward bias (2 V), two peaks were observed at 4.5 ± 0.05 and 9.5 ± 0.05 μm due to transitions from QD ground state to the wetting layer state and to the second QD excited state, respectively. Under reverse bias (-3.25 V), two peaks were observed at 4.9 ± 0.05 and 16.9 ± 0.1 μm due to transitions from QD ground state to the wetting layer state and to the first QD excited state, while the peak at 9.5 μm (observed for forward bias) is not apparent. A summary of peak selec-

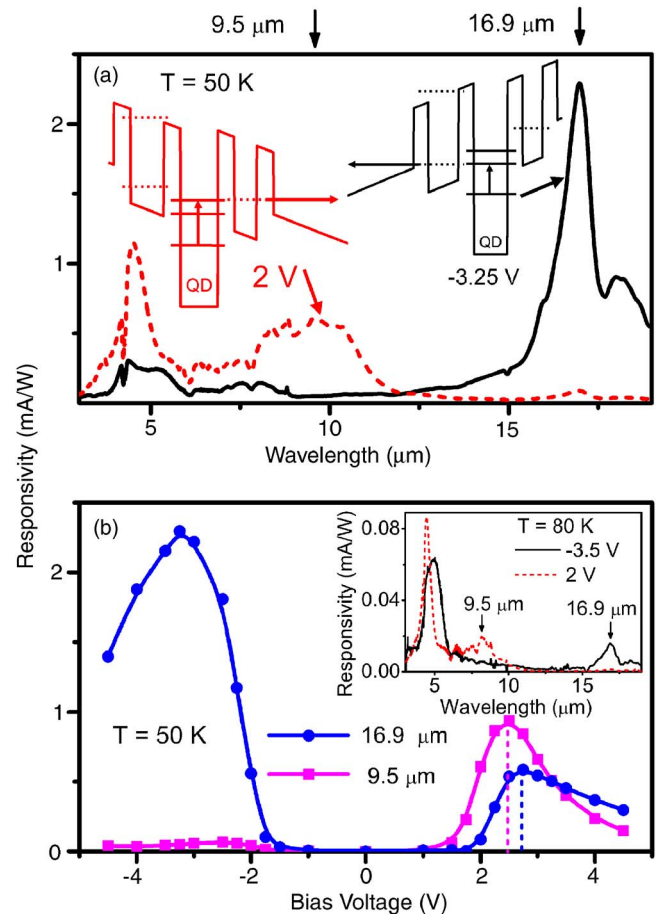


FIG. 3. (Color online) (a) Spectral responsivity of the T-QDIP detector at 50 K under 2 and -3.25 V bias. The energy state alignments under these bias conditions are also shown. (b) Variation of the peak responsivity with applied bias. By alternating the bias polarity, the detector can be operated at 9.5 or 16.9 μm . The peak response becomes maximum when resonant tunneling condition is met for a certain bias value (2 and -3.25 V for 9.5 and 16.9 μm peaks, respectively). Spectral responsivity at 80 K under 2 and -3.5 V bias is shown in the inset.

TABLE I. Selection of wavelength using the applied bias.

Bias (V)	Peak wavelength (μm)		
	4.5/4.9	9.5	16.9
2	✓	✓	
-3.25	✓		✓

tion by using applied bias is given in Table I. The observed peak selectivity is consistent and in good agreement with the theoretical calculations, as explained above. The shift of the peak associated with the wetting layer is also expected and in good agreement with the calculated results. The calculated transition energies (ΔE for transition 1) are 264 and 249 meV for forward bias and reverse bias, respectively. This change is due to the energy shift of the wetting layer state by the applied electric field relative to the QD states. Also, the carriers excited to the wetting layer can escape even under nonresonant conditions since this state is close to the top band edge of the barriers. As compared to the calculated peak positions, the observed peak positions are in reasonably good agreement and any deviation can be associated with the uncertainty in structure parameters (such as material composition, layer thickness in DBs and size of QDs) and the uncertainty in the calculation.

According to the variation of the peak response with applied bias shown in Fig. 3(b), it is clearly evident that there is a specific voltage at which the maximum response for each peak can be obtained. The 9.5 μm peak exhibits its maximum responsivity (0.9 mA/W) at 2.5 V, while the 16.9 μm peak has a maximum responsivity of 3 mA/W at -3.25 V. According to Fig. 2, the voltage at which the maximum peak response appears corresponds to the voltage required ($\pm 3 - \pm 3.5$ V) to level the QD excited states and DB states. When the bias is increased in the reverse direction, only the first QD excited state approaches the state in the BDB, while the second QD excited state deviates. Hence, only the carriers excited to the first QD excited state will undergo resonant tunneling. At -3.25 V bias the 16.9 μm peak is very strong and the 9.5 μm peak is weaker by a factor of 50. However, when the forward bias is increased, both the first and second QD excited states approach the state in the TDB, opening resonant tunneling conditions for carriers excited into both QD states. Consequently, both 9.5 and 16.9 μm peaks are visible under forward bias and the 16.9 μm peak reaches its maximum response for a higher bias voltage than that for the 9.5 μm peak.

The temperature dependence of the response showed that all the peaks with the peak selectivity can be observed up to 80 K [see Fig. 3(b)], while the short peak (4.5–5 μm) can be observed up to 100 K. The dark current densities at 80 and 300 K are $\sim 4 \times 10^{-8}$ A/cm² at ± 4 V and $\sim 8 \times 10^{-4}$ A/cm² at ± 2 V, respectively. This comparatively⁷ low dark current is attributed to dark current blocking by the DBs. The detectivity values at 50 K for the peaks at 4.5 (2 V), 9.5 (2 V), and 16.9 μm (-3.25 V) are 3.0, 1.6, and 6.0×10^{12} Jones, respectively.

Although the present structure shows three peaks with two having bias sensitivity, the DB system provides various design possibilities. For example, as shown in Fig. 4, a modi-

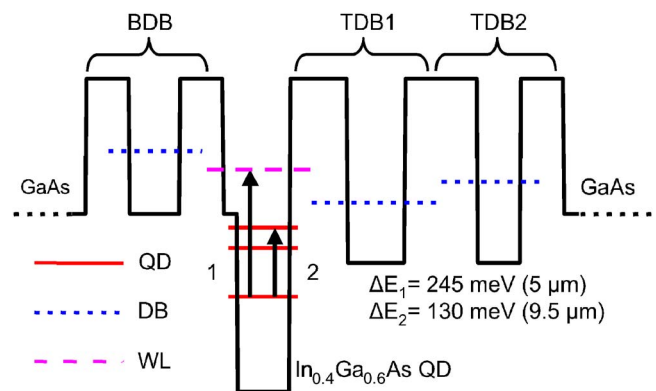


FIG. 4. (Color online) Proposed T-QDIP structure having bias-selectable response peaks only in 3–5 and 8–14 μm atmospheric windows.

fication of the structure to block the photocurrent leading to the 16.9 μm peak and provide resonant conditions for the wetting layer state (under reverse bias) would lead to a dual-band detector with two bias-selectable peaks in 3–5 and 8–14 μm atmospheric windows. This structure uses two TDBs (TDB1 and TDB2), which the excited electrons to the second QD excited state tunnel through via resonant tunneling for forward bias. Two DBs will provide an extra blockade for the carriers excited (under forward bias) into the wetting layer.

This work is supported in part by the U.S. Air Force under the STTR Contract No. FA9550-07-C-0137, AFOSR Grant No. FA9550-06-1-0500, and the U.S. NSF Grant No. ECCS: 0620688.

- ¹A. Goldberg, P. N. Uppal, and M. Winn, *Infrared Phys. Technol.* **44**, 427 (2003).
- ²F. Neele, *Proc. SPIE* **5787**, 134 (2005).
- ³D. B. Law, E. M. Carapezza, C. J. Csanadi, G. D. Edwards, T. M. Hintz, and R. M. Tong, *Proc. SPIE* **2938**, 288 (1997).
- ⁴P. M. Alsing, D. A. Cardimona, D. H. Huang, T. Apostolova, W. R. Glass, and C. D. Castillo, *Infrared Phys. Technol.* **50**, 89 (2007).
- ⁵B. Aslan, H. C. Liu, M. Korkusinski, S. J. Cheng, and P. Hawrylak, *Appl. Phys. Lett.* **82**, 639 (2003).
- ⁶B. Kochman, A. D. Stiff-Roberts, S. Chakrabarti, J. D. Phillips, S. Krishna, J. Singh, and P. Bhattacharya, *IEEE J. Quantum Electron.* **39**, 459 (2003).
- ⁷S. Krishna, G. von Winkel, S. Raghavan, A. Stintz, G. Ariyawansa, S. G. Matsik, and A. G. U. Perera, *Appl. Phys. Lett.* **83**, 2745 (2003).
- ⁸S. D. Gunapala, S. V. Bandara, C. J. Hill, D. Z. Ting, J. K. Liu, S. B. Rafol, E. R. Blazejewski, J. M. Mumolo, S. A. Keo, S. Krishna, Y.-C. Chang, and C. A. Shott, *Infrared Phys. Technol.* **50**, 149 (2007).
- ⁹S. Tsao, H. Lim, W. Zhang, and M. Razeghi, *Appl. Phys. Lett.* **90**, 201109 (2007).
- ¹⁰S. Krishna, D. Forman, S. Annamalai, P. Dowd, P. Varangis, T. Tumolillo, Jr., A. Gray, J. Zilko, K. Sun, M. Liu, J. Campbell, and D. Carothers, *Appl. Phys. Lett.* **86**, 193501 (2005).
- ¹¹F. D. P. Alves, G. Karunasiri, N. Hanson, M. Byloos, H. C. Liu, A. Bezinger, and M. Buchanan, *Infrared Phys. Technol.* **50**, 182 (2007).
- ¹²P. Bhattacharya, X. H. Su, S. Chakrabarti, G. Ariyawansa, and A. G. U. Perera, *Appl. Phys. Lett.* **86**, 191106 (2005).
- ¹³F. Pulizzi, D. Walker, A. Patané, L. Eaves, M. Henini, D. Granados, J. M. Garcia, V. V. Rudenkov, P. C. M. Christianen, J. C. Maan, P. Offermans, P. M. Koenraad, and G. Hill, *Phys. Rev. B* **72**, 085309 (2005).
- ¹⁴K. K. Choi, B. F. Levine, C. G. Bethea, J. Walker, and R. J. Malik, *Phys. Rev. Lett.* **59**, 2459 (1987).
- ¹⁵X. Su, S. Chakrabarti, P. Bhattacharya, G. Ariyawansa, and A. G. U. Perera, *IEEE J. Quantum Electron.* **41**, 974 (2005).
- ¹⁶H. Jiang and J. Singh, *Phys. Rev. B* **56**, 4696 (1998).
- ¹⁷E. Anemogiannis, N. Glytsis, and T. K. Gaylord, *IEEE J. Quantum Electron.* **33**, 742 (1997).